



Research papers

Compressed air energy storage with T100 microturbines: Dynamic analysis and operational constraints

M. Raggio^{*}, M.L. Ferrari

Thermochemical Power Group (TPG), Dipartimento di Ingegneria Meccanica, Energetica, Gestionale e dei Trasporti, Università degli Studi di Genova, Italy



ARTICLE INFO

Keywords:

Compressed air energy storage
Micro gas turbines
Transient analysis
Surge margin

ABSTRACT

The aim of this paper is the dynamic analysis of a small-size second-generation Compressed Air Energy Storage (CAES) system. It consists of a recuperated T100 micro gas turbine, an intercooled two-stage reciprocating compressor and an artificial tank for air storage. The possibility of including an innovative air expander before the injection into the turbine is also investigated. Starting from background on design and management optimization, this work proposes dynamic simulations and definition of operational constraints, not considered in previous publications. These represent significant results to extend the system range (producing efficiency and cost benefits), avoiding risks and failures in prototypes as well as in commercial applications. Following a section with calculations motivating the activity from an economic point of view, the interaction of the T100 integrated with the CAES system is analysed through a validated dynamic model. Close attention is paid to the discharging of the air storage vessel because the increment of mass flow at the turbine expander can lead to surge margin decrease and thermal stresses, especially during dynamic operations. Consequently, maximum limits for the air injection are obtained and different operational strategies are considered to ensure safe operation during the system dynamics, enlarging the application range or proposing modifications in the control system.

1. Introduction

In recent years the installation of renewable energy sources (RESs), mainly solar and wind power, has significantly increased as a means of producing clean energy and overcome the detrimental effects associated with fossil fuel utilisation, such as climate change, air pollution, and depletion of finite resources [1]. Despite these benefits, the implementation of RES brings various obstacles. For instance, their weather dependence leads to daily and seasonal unpredictable and intermittent power production. Therefore, traditional fossil fuel-based generators are still needed to produce consistent and reliable energy. Moreover, they must operate at part-load for a longer time, provide faster run-up and undergo more frequent shutdowns, leading to less efficient energy conversion and increased emissions [2,3]. Consequently, an evolution of grid integration, forecasting, and storage technology is required to support a deeper penetration of renewables and reduce the dependency on fossil fuels [4–6].

Nevertheless the power system network structure is also changing for the increasing installation of more distributed energy resources (DERs) [7]. Some of the DERs benefits are the better exploitation of RES and

other energy-efficient solutions such as combined heat and power (CHP) units, reduced transmission losses, increased control and energy security for local communities, provision of electricity in remote rural areas and cost-effectiveness for small-scale projects [8]. Distributed prime movers, with different characteristics, both programmable and non-programmable, can be grouped in microgrids (MGs) to combine their benefits and exploit all their potential [9]. However, the integration of microgrids into the existing grid infrastructure comes with several challenges on the management of generators with different requirements, especially if the microgrid includes CHP units, which are required to satisfy not only the electrical demand but also the thermal needs of a nearby district heating network (DHN). These criticalities make energy storage systems (ESSs) essential for microgrids efficient operation. ESSs can help balance mismatches between electricity supply and demand, optimising the use of distributed energy sources for efficient energy use and decoupling electrical and thermal energy production in case of CHP plants [10]. In addition, energy storage systems can also improve the reliability and resiliency of the grid when employed as backup power during possible outages [11].

Among different ESSs [12], the compressed air energy storage

^{*} Corresponding author.

E-mail address: martina.raggio@edu.unige.it (M. Raggio).

(CAES) systems are cost-effective, highly flexible and with a low environmental impact compared to other storage devices, such as batteries, as being free from toxic or flammable materials [13]. In CAES systems, the air is compressed and stored in a storage device during off-peak hours and later expanded into a turbine during peak demand. Large CAES plants must be located near underground caverns since significant storage volumes are needed on account of the low energy density of compressed air. These geological constraints do not necessarily affect small-size CAES systems that can alternatively employ artificial above-ground tanks. Distributed CAES is also suitable for cogeneration or tri-generation, as a consequence of the heating and cooling power obtained during compression and expansion [14–16]. In addition, the lower capital and installation costs of small-size CAES systems make these systems more accessible to a broader range of customers [17].

Regardless of size, traditional compressed air energy storage (CAES) systems can be classified based on the compression method into three main categories: diabatic (D-CAES), adiabatic (A-CAES), and isothermal (I-CAES) systems. D-CAES systems dissipate the heat generated during compression into the environment. While relatively simple and affordable, this method results in lower efficiency and requires some fuel to feed the combustion process to pre-heat the air before the expansion [18]. On the other hand, A-CAES systems utilise thermal energy storage (TES) systems to store the heat generated during compression and use it in the expansion process. This results in improved efficiency and eliminates the need for combustion at the expense of increased complexity [19]. Finally, I-CAES systems aim to eliminate the need for combustion and TES by reaching nearly isothermal compression through different techniques. The most common solutions investigate the possibility of using liquid pistons, manipulating the compressor chamber geometry, spraying liquid or foam droplets into the compression chamber, or combining both. Despite the numerous studies available in literature [20,21], these solutions are limited by slow compression and expansion processes and are not yet ready for the marketplace.

This paper investigates an alternative option, named second-generation CAES (S-CAES), where the compression and storage systems are integrated with a standard micro gas turbine (mGT), instead of fully decoupling compression and expansion [17,22,23]. In this solution, the air is compressed externally and then, when required, discharged downstream of the mGT compressor. During the injection phase, for the same power output, the mGT compressor elaborates a lower mass flow than regular operation, reducing the compressor work and fuel utilisation. Along with the reduced fuel consumption, air injection can also be used to increase the maximum mGT power output [17]. Micro gas turbines are highly efficient energy systems for CHP applications with several advantages such as fast response, low noise/vibration levels, fuel flexibility and modularity [24]. Although still relying on fossil fuels, this system can continuously operate and satisfy the energy demand even when the storage vessel is empty. Moreover, micro gas turbines are potentially fuel-flexible and alternative fuels, such as hydrogen or e-fuels, could be used in the future [25,26] in combination with CAES systems (to exploit the benefits of these technologies). Despite reliability and flexibility, the S-CAES mass flow discharge rate is limited by the specific mGT capabilities to handle an increased mass flow rate at the expander. These limitations are mainly related to the structural limits of the machine, combustion performance, possible thermal gradients and compressor instabilities. Specifically during transients, thermal gradients and reduced surge margin [17,22] can decrease the system flexibility and limit the mGT operating conditions.

Most published works on small-size CAES focus on design optimisation, techno-economic analysis and energy management within microgrids [27–29]. In addition, few analyses have been performed on second-generation small CAES systems. Salvini [17] studied an S-CAES system based on a 4600 kW Mercury recuperated gas turbine, demonstrating that a 30 % maximum power augmentation can be obtained during the discharging phase with the safe operation of the machine.

Arnulfi [22] considered a 100 kW mGT with a similar S-CAES configuration, estimating the maximum mass flow that could be injected in the mGT. Both these studies were based on steady-state off-design models, neglecting the time-dependent performance and constraints. Some dynamic studies have been carried out, but mainly concerning A-CAES systems. Jin et al. [30] considered an A-CAES used to reduce fluctuations generated by wind power production. Mucci et al. [31] analysed different control strategies to increase the system performance during off-design conditions by regulating the compressor speed and the throttling valve opening during the charge phase. However, analysis on small-scale second-generation CAES transients has never been conducted.

This paper aims to fill in the gap in the dynamic analysis of small-size S-CAES systems by investigating the effects of air injection during the CAES discharging phase on transient operating issues (mainly thermal gradients and compressor stability issues) and analysing the risky operating conditions. Presented here is an activity concerning a commercial microturbine (the AE-T100) extending its application range considering the integration with the CAES system. For this reason, the results obtained in this work can have fast commercial application in real CAES/mGT plants with an important positive impact for sustainable energy generation coming from average efficiency increase of a system suitable either for alternative fuels (e.g., biogas, hydrogen [32], etc.) or applications in concentrated solar systems [33]. This is an important innovation considering that the most recent papers on CAES systems in dynamic conditions refer to large plants connected with caverns [34] (in some cases with compressing and expanding systems operating on different shafts [35,36]) and the attention is mainly related to the charging/discharging dynamics [37]. When the surge margin limitation is taken into account (e.g., in [38]), no specific dynamic results are reported and since compressors and turbines are on different shaft, results are not able to cover the air injection issues in a commercial microturbine. Moreover, the paper in [36] proposed an interesting and complex layout, but with different integration aspects and dynamics in comparison with the system analysed here with an AE-T100 micro gas turbine. Another significant innovation concerns the proposed integration with the Tesla turbine technology [39,40] as a topping expander to recover additional work before the injection. This analysis was performed in TRANSEO, a dynamic tool developed by the Thermochemical Power Group (TPG) based on validated components for transient/dynamic calculations on energy systems, using the MATLAB/Simulink interface [41].

2. Plant layout

The plant layout considered in this work (an AE-T100 mGT coupled with the external CAES system as shown in Fig. 1) is not fully innovative because it was already considered in Arnulfi et al. [22]. The innovative part from the layout point of view regards the application of a Tesla turbine to exploit the expansion for the air flow injected in the microturbine. However, the main innovation of this work involves the dynamic analysis and the identification of constraints related to the system dynamic behaviour (mainly related to the surge margin and the thermal stress of the microturbine system). The AE-T100 is a recuperated micro gas turbine for CHP applications, providing up to 100 kW_{el} of electrical power and 165 kW_{th} of thermal power at design conditions. The nominal electrical efficiency is 30 % and the total cogenerative efficiency is 80 %. The control system maintains the Turbine Outlet Temperature (TOT) constant and equal to 645 °C. This TOT value ensures a good electrical efficiency – typical of similar-sized mGTs - while preserving the recuperator life, sensitive to high temperatures and thermal gradients. The turbine operating power range is 20 kW_{el}–100 kW_{el}. The mGT main specifications at full load are summarised in Table 1 and are referred to an ambient temperature of 15 °C [42].

The CAES side consists of a two-stage reciprocating compressor (85 % isentropic efficiency) with intercooling (89 % effectiveness) and

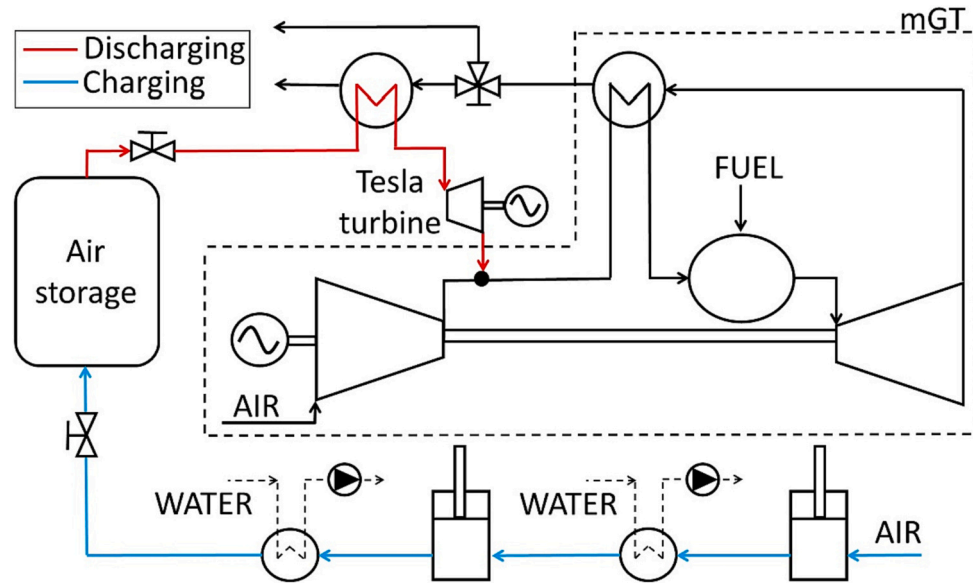


Fig. 1. Plant Layout.

Table 1
AE-T100 mGT design point specifications.

Specification	Value	Unit
Electrical power	100	kW
Thermal power	165	kW
Electrical efficiency	30	%
Overall cogeneration efficiency	80	%
Pressure ratio	4.5	-
Rotational speed	70,000	rpm
Turbine outlet temperature	645	°C

aftercooling (87 % effectiveness) using water as a cooling medium (charging side), an artificial vessel (storage side), a small-size Tesla turbine and an additional recuperator for the air pre-heating (discharging side). Surplus electricity from renewable sources or low-price electricity can be used to compress the air by means of the reciprocating compressor. Subsequently the air is stored until the discharge phase, where the air heats up and expands before being injected upstream of the T100 recuperator. The main CAES system design point specifications are reported in Table 2.

A two-stage compressor represents a trade-off between compressor efficiency and cost. Therefore, a relatively low tank maximum pressure of 50 bar has been chosen, in agreement with a previous off-design study from Arnulfi et al. on a similar layout [22]. On the discharging side, two options, both considered, are possible: 1) a direct injection into the mGT or 2) an expansion prior to the injection. In the former case the obtained fuel savings is only due to the reduced compressor work; in the latter case additional fuel can be saved by recovering additional work from the pressure difference between the tank outlet and mGT injection point. In this application the minimum allowed outlet pressure of the turbine is set to 4.5 bar, which is higher than the maximum pressure supplied by the T100 compressor in the considered operating points (as presented in

Table 2
CAES system design point specifications.

Specification	Value	Unit
Tank maximum pressure	50	bar
Compressor isentropic efficiency (equal for each stage)	85	%
Tesla isentropic efficiency	30	%
Intercooler effectiveness	89	%
Aftercooler effectiveness	87	%

Paragraph 4). In both cases, air pre-heating is always required to avoid temperatures close to or below 0 °C, which could cause freezing problems. Due to its size, a Tesla turbine is a more suitable device for being employed as an expander into micro power generation applications compared to traditional devices. In detail, it is a bladeless turbine that uses discs to exploit the adhesion and friction created by the working fluid. Good isentropic efficiencies can be reached, as demonstrated in different experimental studies [39,40]. However, in this work an isentropic efficiency equal to 30 % is considered to obtain results based on the state-of-the-art of Tesla expanders, not on the latest results to be confirmed by further analyses.

3. Model assumptions and validation

The T100 and CAES system were modelled with the TRANSEO software, a library of modular components for modelling energy systems dynamics, developed in the MATLAB/Simulink platform. Many previous studies have validated all the available components and the interconnecting approach [43–45]. According to its interconnecting logic, defined as “mass continuity” logic, each component receives the mass flow rate information from either the upstream or downstream connected component. Concurrently the pressure is calculated internally, depending on the component physical characteristics and the calculated value is sent in the opposite direction of the mass flow. The behaviour of energy systems can be primarily determined by mass and energy balances. The impact of the momentum balance, such as the phenomena of pressure wave propagation, can typically be neglected due to faster timescales. Most TRANSEO components are modelled according to a “lumped-volume” representation to ensure a good balance between accuracy and calculation speed. A more detailed but still simplified approach is the “quasi 2D approach”, which involves discretising the components into the flow direction to model the heat transfer effects between adjacent cells. This level of detail is required in components such as the recuperator, where the heat transfer phenomena need to be modelled more accurately. As a consequence, the model is developed using a library of components that are interconnected as shown in [41,45]. No convergence algorithm is implemented because the results are obtained in time-dependent mode from the interactions between the components. In the AE-T100 machine, for instance, mass flow rates are calculated by the compressor and the expander (with the related maps), while pressure is calculated by the plenum included between the compressor and the recuperator (all in time-dependent mode),

considering also the impact on pressure by the other components (e.g., the recuperator, etc.).

In addition to validating the single components, TRANSEO has shown accurate predicting behaviour for modelling micro gas turbines in various configurations [43,44,45–47]. In particular, the T100 micro gas turbine has been investigated in different layouts such as solar-hybrid configurations [44], humidified cycles [48] and injection of compressed air [49]. The T100 model used in this analysis was validated in a previous study [47], where the experimental activities performed to validate the model were conducted on a Turbec T100 (now with the name AE-T100) of the Vrije Universiteit Brussel (VUB) facility. This specific T100 was modified to be also used in a humidified cycle, but in this work only the standard dry operation is considered. The model was validated up to 85.8 kW at 25 °C for steady-state and dynamic conditions. The results matched well the experimental data, with errors below 1.5 %, lower than the sensors accuracy range. The same model has been successfully validated, showing good matching by injecting compressed air in the T100 in the steady-state and dynamic behaviours [47]. The additional components (reciprocating compressor, heat exchangers, artificial tank and Tesla turbine) of the CAES system have been included in this model.

3.1. Lumped-volume approach

The components modelled according to the “lumped-volume” approach are pipes, compressor, turbine, combustor and storage tank. According to this modelling approach [41], the component calculations are performed by superimposing two effects that determine first 1) the steady-state off-design performance and then 2) the dynamic behaviour by modelling the component as a duct of equivalent cross-sectional area (A_{eq}) and length (L_{eq}). The off-design behaviour of each component is dependent on the internal characteristics. For example, the piping system steady-state behaviour is modelled as a pressure drop, according to Eq. (1):

$$\Delta p_{pipe} = \rho \frac{v^2}{2} f \frac{L_{eq}}{D_{eq}} \quad (1)$$

where ρ and v are the density and fluid velocity, f is the friction coefficient and D_{eq} is the duct equivalent diameter.

The transient behaviour of the “lumped-volume” components can be determined using the momentum and energy equations, numbered from (2) to (4):

$$\frac{d\dot{m}}{dt} = \frac{A_{eq}}{L_{eq}} (C - \Delta p) \quad (2)$$

$$\frac{d(c_v \rho V T)}{dt} = \dot{m} \Delta h - \dot{q}_{solid} \quad (3)$$

$$\frac{d(c_{p,solid} M_{solid} T_{solid})}{dt} = \dot{q}_{solid} - \dot{q}_{loss} \quad (4)$$

where the momentum contribution from the actuator is represented by C , the pressure and enthalpy difference of the fluid between the duct inlet and outlet are represented by Δp and Δh respectively, \dot{q}_{solid} represents the heat flux through the solid duct part, including the thermal power heating the metal and the heat lost to the environment. Each component solves Eqs. (2) to (4) and the additional characteristic steady-state equations. The equivalent duct is not divided into discretised segments; therefore, its equations are only integrated over time and not along its length.

3.1.1. Compressor and turbine

The compressors and turbines are represented by 0-D non-dimensional characteristic maps, where the non-dimensional mass flow and efficiency are determined from the corrected rotational speed

and pressure ratio. This allows calculating the total outlet temperature through isentropic relations (Eqs. (5) and (7)) and, therefore, the power produced or consumed (Eqs. (6), (8)), respectively.

The main compressor equations to calculate the outlet total temperature $T_{compr-out}$ and absorbed power P_{compr} are reported below:

$$T_{compr-out} = T_{compr-in} \left(1 + \frac{\beta_{compr}^{\frac{\gamma-1}{\gamma}} - 1}{\eta_{compr}} \right) \quad (5)$$

$$P_{compr} = \dot{m}_{compr} c_{p-mean} (T_{compr-out} - T_{compr-in}) / \eta_m \quad (6)$$

where $T_{compr-in}$ is the compressor inlet total temperature, β_{compr} is the compressor pressure ratio, η_{compr} the isentropic efficiency, γ is the ratio of the specific heats at constant pressure and volume, \dot{m}_{compr} is the compressor mass flow, c_{p-mean} the compressor average specific heat and η_m is the mechanical transmission efficiency, which is 0.99 in this case.

Similarly, the turbine equations to calculate the outlet total temperature $T_{turb-out}$ and the generated power P_{turb} are reported below:

$$T_{turb-out} = T_{turb-in} \left[1 - \eta_{turb} \left(1 - \beta_{turb}^{\frac{\gamma-1}{\gamma}} \right) \right] \quad (7)$$

$$P_{turb} = \dot{m}_{turb} c_{p-mean} (T_{turb-in} - T_{turb-out}) \quad (8)$$

where $T_{turb-in}$ is the turbine inlet total temperature, β_{turb} is the turbine expansion ratio, η_{turb} the isentropic efficiency, γ is the ratio of the specific heats at constant pressure and volume, \dot{m}_{turb} is the turbine mass flow and c_{p-mean} the turbine average specific heat.

The heat transfer calculation considers of the compressor and turbine heat exchange, along with the heat lost to the environment.

3.1.2. Combustor

For the combustor, the off-design behaviour is described by solving the unsteady energy equation (Eq. (9)), considering the combustion efficiency $\eta_{comb} = 0.996$ and methane LHV = 43.44 MJ/kg:

$$\frac{d(c_v \rho_{mean} V T_{out})}{dt} = \left(\dot{m}_{air} h_{air} \right)_{in} + \dot{m}_{fuel} h_{fuel} + \dot{m}_{fuel} \eta_{comb} LHV - \left(\dot{m}_{gas} h_{gas} \right)_{out} \quad (9)$$

$$\dot{m}_{gas} = \dot{m}_{air} + \dot{m}_{fuel} \quad (10)$$

where, c_v is the specific heat at constant volume, ρ_{mean} is the mean density, V is the volume, T_{out} the combustor outlet total temperature, \dot{m} is the fluid mass flow rate and h the enthalpy; the subscript “air” is referred to the inlet air properties, “fuel” to the fuel properties and “gas” to the exhaust gas, whose mass flow is calculated according to Eq. (10).

The pressure losses in the combustor are calculated considering the contribution of viscous losses and pressure drops due to the fluid acceleration.

3.2. Quasi-2D approach

The recuperators and heat exchangers are modelled using a quasi-2D approach [41]. This approach involves a discretisation of the component to model the unsteady form of the energy equation. By contrast the continuity and momentum equations are calculated according to the simplified “lumped-volume” approach in one single cell. This is a reasonable assumption considering the low flow velocity involved in the heat exchanger (around 10 m/s).

3.2.1. Recuperator

The recuperator is a counter-flow heat exchanger used to heat up compressed air using the hot stream of exhaust gases leaving the turbine at ambient pressure. The discretisation is shown in Fig. 2, where the component is vertically divided into four main parts, identified by the

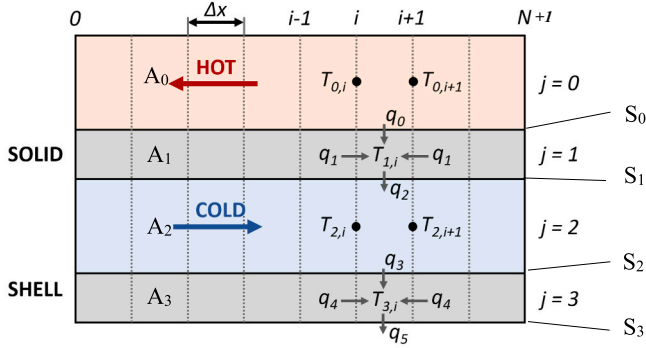


Fig. 2. TRANSEO heat exchanger discretisation.

subscript “j”, representing the hot and cold flow passages, the internal matrix, and the external vessel. Each main part is then longitudinally discretised into N elements to improve the calculation accuracy of the dynamic energy and heat transfer equations, where “i” refers to the i-th element in the discretisation. The following energy Eq. (11) is solved according to a partial difference numerical scheme:

$$\rho_{j,i} c_{v,j} A_j \frac{\partial T_{j,i}}{\partial t} = -c_{p,j} \dot{m}_j \frac{\partial T_{j,i}}{\partial x} + \dot{q}_{j,i} \quad (11)$$

where the heat source $\dot{q}_{j,i}$ includes factors such as convection between solid walls and fluids, heat losses to the environment and conduction along the longitudinal axis of the heat exchanger. The components of $\dot{q}_{j,i}$ are calculated using standard conductive and convective heat transfer equations based on the parameters and physical properties specified by the specific heat exchanger. The surfaces A_j represent the total cross-sectional areas of each cell, while the surfaces S_j represent the portion of the exchanging surface relative to each cell.

3.3. Other components

The other components that do not belong to the “lumped-volume” and “quasi-2D” categories are the tank volume, the T100 shaft and control system.

3.3.1. Storage tank

The tank volume integrates continuity and energy equations to determine its internal pressure and temperature based on the mass flow information from upstream and downstream and considering the heat loss to the environment. The unsteady continuity and energy equations (Eqs. (12), (13)) are reported below:

$$\frac{d(\rho V)}{dt} = \dot{m}_{in} - \dot{m}_{out} \quad (12)$$

$$\frac{d(\rho VT)}{dt} = \frac{c_{p-out}}{c_v} \left(\dot{m}_{in} T_{in} - \dot{m}_{out} T_{out} \right) \quad (13)$$

The outlet temperature T_{out} for the following time step is calculated from Eq. (13) while the continuity equation of Eq. (12) is used to update the tank mass flow.

3.3.2. Shaft

The T100 shaft is the link between compressor, turbine, and generator; it transfers the mechanical power produced by the turbine to the generator, where it is transformed into electrical power. The rotational speed of the shaft is determined by Eq. (14), considering the effect of the turbocharger rotational inertia J and the mechanical power losses in bearings:

$$P_{turb} - P_{compr} - P_{loss} = J \frac{d(\omega^2/2)}{dt} \quad (14)$$

where P is the power, ω is the rotational speed.

3.3.3. Control system

The T100 model control system integrates two control loops [41] to deliver the required power output and maintain the TOT value equal to the setpoint of 645 °C. The first loop is for controlling the electrical power output using a feedforward and a slow PI technique. In this loop the set point value of the rotational speed is obtained by combining the effects of the feedforward approach based on a predefined table and the PI controller, which receives the TOT as input. The second loop employs a fast PID controller to manage the fuel valve opening and keep the TOT equal to 645 °C.

4. Steady-state results

This steady-state analysis intends to investigate the behaviour of the micro gas turbine when stable part-load conditions are reached during constant air injection. The results presented in this section were calculated with the dynamic model presented in the previous section waiting for stable conditions for each operating point. The main steady-state performance parameters were obtained with an ambient temperature of 25 °C for electrical power outputs in the 40 kW–80 kW range (since the model was validated up to 85.8 kW), imposing different values of injected compressed air at 25 °C. These values are presented in Table 2.

The compressor stability is the main limiting factor for the maximum amount of air that can be injected upstream of the compressor. The surge margin “ k_p ” is commonly used in literature to measure the safety of an operating point from a surge event, although various definitions exist. In this work, the surge margin is indicated with k_p and it is calculated using Eq. (15) [49]:

$$k_p = \frac{\dot{m}_j \beta}{\dot{m}_{s.l.} / \beta_{s.l.}} \quad (15)$$

where the subscript “s.l.” means that the respective value is calculated where the iso-speed line intersects the surge line of the considered operating point. According to the definition, the theoretical minimum limit for the surge margin should be 1, but it is advisable to maintain a safety margin to mitigate potential risks from minor fluctuations in the system. Following previous studies [49], a surge margin of 1.1 is considered the lower limit for this analysis.

During steady-state conditions, when working at constant net power output P_{net} and fixed TOT, the injection of air upstream of the compressor reduces the required compression work. Therefore, the turbine subtracts less power and requires less fuel flow, increasing the electrical efficiency. At the same time, the rotational speed, compressor mass flow and pressure ratio decrease, bringing the new operating point closer to the surge line. Since the regular operating points of the T100 at higher P_{net} have a higher surge margin, more air can be injected in those conditions compared to lower P_{net} conditions. Fig. 3 shows the surge margin for different P_{net} and \dot{m}_{inj} while Fig. 4 displays the maximum mass flow that can be injected as a function of P_{net} for this specific machine. Steady-state results help identify the limits during stable operations. Consequently, these results are an important guide for designing the CAES/mGT integration extending the operative range of this commercial machine to the maximum operating limits and to avoid risk of failures. However, during transient variations, there could be operating conditions leading to potential compressor instability even when the injected mass flow is within the acceptable ranges in steady-state conditions. Therefore, a dynamic analysis is essential to evaluate the effective constraints to be considered in a real implementation.

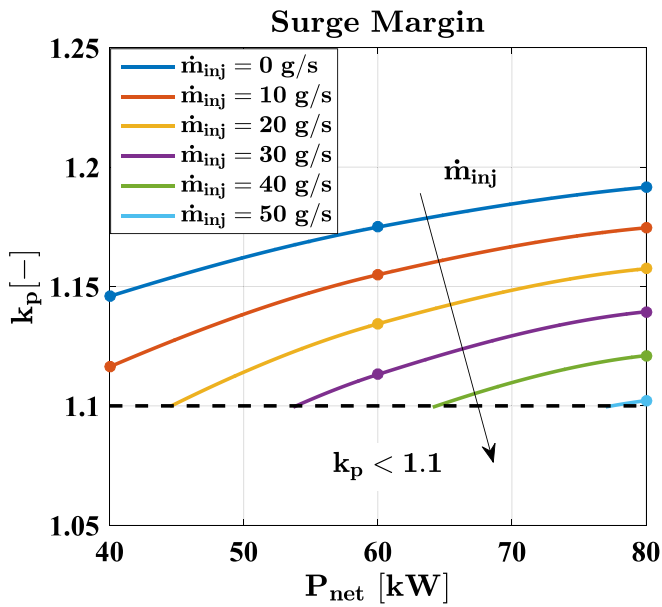


Fig. 3. Surge margin for different P_{net} and \dot{m}_{inj} .

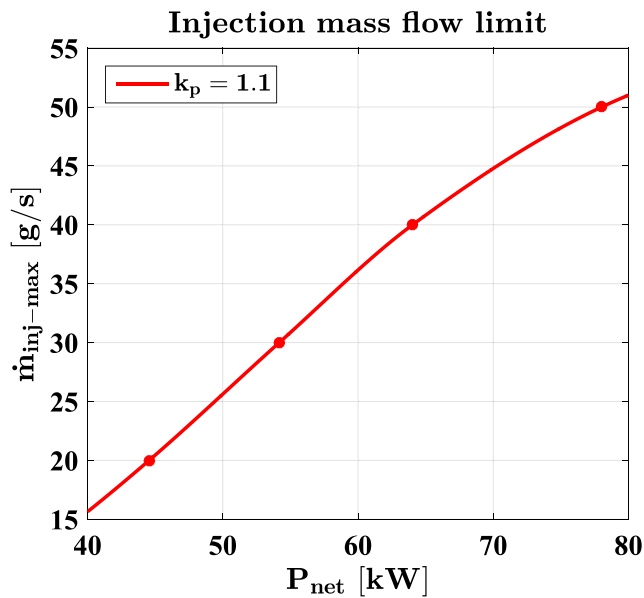


Fig. 4. Maximum injectable mass flow as a function of P_{net} .

The most significant benefits in terms of increased electrical efficiency can be obtained by injecting air at higher P_{net} since the starting η_{el} is higher and more air can be injected due to the higher surge margin in standard operation. For example, by injecting the same air mass flow rate of $\dot{m}_{inj} = 10$ g/s, at the low power output of $P_{net} = 40$ kW, the electrical efficiency increases by +0.51 %, and at the higher power output of $P_{net} = 80$ kW, the electrical efficiency increases by +0.74 % in absolute terms. In addition, at $P_{net} = 40$ kW the maximum increment of η_{el} is +0.76 % when $\dot{m}_{inj} = 15$ g/s, while at $P_{net} = 80$ kW the maximum increment is +3.23 % at $\dot{m}_{inj} = 50$ g/s.

The results shown on Table 3 were obtained by injecting air at constant ambient temperature ($T = 25$ °C), although during transient operation the compressed air temperature can vary depending on the tank temperature, as well as on conditions of the heat exchanger used for the pre-heating and possible presence of the Tesla turbine. Injecting air at ambient temperature lowers the compressor outlet temperature by approximately between 2 and 4 °C every 10 g/s of injected air due to the mixing with colder air. However, the recuperator can provide almost the same outlet temperature on the cold side (with a negligible variation of 0.1–0.3 °C every 10 g/s of injected air). Therefore, the impact of possible temperature variations of the compressed air on the electrical efficiency is negligible and compressed air temperature reductions do not affect the electrical efficiency. However, this effect causes a reduction of around 5 °C every 10 g/s of injected air on the recuperator outlet temperature on the hot side, whose effect should be considered in determining the reduced thermal power. The results reported here are a good mapping of this CAES/mGT coupling with important impact on real system development and optimization. For instance, the efficiency and fuel consumption change can be used to develop a simplified model (e. g., based on lookup tables) for the interaction with an optimization algorithm.

5. Motivation for the dynamic analysis

As previously presented the aim of this paper regards the dynamic analysis related to the impact of the CAES system on the AE-T100 microturbine, focusing special attention on the constraints that in dynamic mode affect the operating range. Therefore, no optimization or management tools were developed and no optimal operating results were obtained. However, to motivate this dynamic analysis a simple calculation is presented showing that the application of this CAES system can produce cost savings also in simple configurations.

Since the AE-T100 operating range is 20–100 kW for the electrical generation point of view and the extreme values are affected by further limitations in the compressor surge margin, a simple scenario was defined considering a low load of 40 kW for the first 12 h (representative of off-peak hours) and 80 kW at a higher load for the remaining 12 h (representative of core hours). The first 12 h could represent night-time

Table 3
Summary of the main steady-state performance points varying P_{net} and \dot{m}_{inj} .

P_{net} [kW]	\dot{m}_{inj} [g/s]	η_{el} [%]	\dot{m}_{fuel} [g/s]	N [rpm]	β_{compr} [-]	$T_{compr,out}$ [°C]	$T_{rec,cold,out}$ [°C]	$T_{rec,hot,out}$ [°C]
40	0	19.28	4.774	60,911	3.295	172.7	601.6	209.8
40	10	19.79	4.652	60,345	3.242	170.3	601.6	205.0
40	15	20.04	4.594	60,077	3.216	169.2	601.7	202.6
60	0	23.43	5.894	64,885	3.763	192.3	601.6	227.1
60	10	23.93	5.770	64,265	3.702	189.8	601.7	222.3
60	20	24.45	5.648	63,664	3.641	187.4	601.8	217.5
60	30	24.98	5.528	63,071	3.581	184.9	601.9	212.8
80	0	24.84	7.412	69,515	4.363	215.7	597.0	245.6
80	10	25.58	7.198	68,702	4.265	211.8	597.4	240.1
80	20	26.26	7.013	67,934	4.181	208.6	597.7	235.1
80	30	26.90	6.844	67,264	4.105	205.7	597.9	230.3
80	40	27.48	6.700	66,703	4.042	203.3	598.1	225.8
80	50	28.07	6.559	66,153	3.979	200.9	598.3	221.3

hours, for example, starting from 20:00 pm to 8:00 am, and the remaining hours from 8:00 am to 20:00 pm of daytime hours. This is a simple scenario different from reality, but useful to highlight a case with an obvious positive impact of the CAES system. Consequently, the results proposed in this section are reported to motivate the following dynamic analysis; for real optimization activities attention can be focused either on the paper by Arnulfi et al. [22] or on future works.

The following possible configurations were considered for comparison (also summarised in Table 4):

1. The mGT alone satisfies the power demand; this case represents the baseline used for comparison against different CAES operations.
2. The plant consists of the mGT and small-size CAES charged during the night-time and discharged during the daytime – without Tesla (2) and with Tesla turbine (2-T).
3. The plant consists of the mGT and small-size CAES charged during the daytime and discharged during the night-time – without Tesla (3) and with Tesla turbine (3-T).

The chosen configurations were selected to compare two cases where the air is injected respectively at a higher load (80 kW) and lower load (40 kW). The selected injected mass flow rates are the maximum limits obtained from the steady-state analysis (to avoid not acceptable injected flows due to the surge limitation): if the discharge occurs during the daytime at $P_{net} = 80$ kW, the maximum mass flow considered in this evaluation is $\dot{m}_{inj} = 50$ g/s, while if the discharge occurs during the night-time at $P_{net} = 40$ kW, the maximum mass flow used here is $\dot{m}_{inj} = 15$ g/s. These numbers are considered to propose simple motivation results and a future work could be developed to optimize them considering real power demand trends. The other goal of this comparison is to estimate the additional beneficial effect including a Tesla turbine.

For cases 2 and 2-T (see Fig. 5), the volume of the tank chosen is 40 m³ to reach the maximum pressure of $p_{max} = 50$ bar during the charging time within the first 12 h, when compressing the constant mass flow $\dot{m}_{charge} = 50$ g/s, equal to the discharged mass flow. At $t = 12$ h, when the electrical demand increases from 40 kW to 80 kW, the mGT ramps up to satisfy the higher load and the injection starts after 15 min. The discharge stops when the tank reaches the minimum allowed pressure of $p_{min} = 4.5$ bar. The Tesla turbine recovers additional power when used, reducing the mGT required power production.

For cases 3 and 3-T (see Fig. 6), the chosen volume is smaller (12 m³) since the mass flow during the charge $\dot{m}_{charge} = 15$ g/s is lower and the comparison between cases is made by considering the same maximum tank pressure ($p_{max} = 50$ bar). In this scenario, at $t = 0$ h, the tank is fully pressurised at 50 bar and the discharging phase starts 15 min after the start of the scenario. Furthermore, in this case, the Tesla turbine grants an additional energy recovery. The discharging phase stops some minutes before reaching 12 h when the tank reaches p_{min} . At $t = 12$ h, the mGT ramps up to provide 80 kW and at the same time the reciprocating

compressor starts to charge the storage volume where the air will be used the following day.

The analysis of the different energy consumptions of these configurations, displayed in Fig. 7, shows that thermal energy provided by the fuel $E_{th-used}$ can be saved when coupling the mGT with a CAES system at the expense of a higher electrical energy $E_{el-used}$ required to run the compressor to charge the tank. Additionally, the Tesla turbine provides further fuel savings as the mGT provides less power compared to the case without the Tesla expander. The results reported in Fig. 7 regard the simple scenario presented in this section with the aim to motivate the importance of the dynamic analysis also from economic point of view. An optimization of the system management (to be performed in future works) could reduce both energy and fuel consumptions. However, this is not related to the dynamic analysis objectives and could be an interesting topic for a future work.

Defining the electrical source for running the compressor while charging is required to estimate the potential economic benefits. In this study, it is considered that the CAES system could be charged in two different ways by using the following:

1. Purchased electrical energy from the grid.
2. Excess of electrical energy from renewable sources.

When purchasing electrical energy from the grid, there are no issues related to the availability of the energy, and the charging can be done at any time of the day. Nevertheless, the availability of renewable energy sources depends on the weather conditions. Therefore, the charging during the day (cases 3 and 3-T) could be done by both wind and solar energy, while the charging during the night (cases 2 and 2-T) is possible by wind sources only. Below, the two cases are considered.

5.1. Electrical energy for the storage charge taken from the grid

Table 5 includes the average costs of natural gas and electricity for the year 2022 (first semester) for three European countries (Italy, Moldova and Sweden) taken as examples [50,51]. These countries are considered for these evaluations to compare a case with high electricity price (Italy) with countries with lower cost for electricity but with different prices for the natural gas (high in Sweden and low in Moldova).

Table 6 displays the daily fuel cost, daily electricity cost, daily earnings, total daily cost, daily savings, and relative daily savings compared to the baseline for each case in each country. These results were obtained by combining the energy consumption results of Fig. 7 and the electricity and natural gas costs of Table 5. For the scenario presented here, the CAES system leads to money savings when the daily and relative savings are positive. The savings are also graphically reported in Fig. 8. This configuration can provide economic savings in countries such as Moldova and especially in Sweden, where the fuel cost is high relatively to the electricity cost (Table 6). On the contrary, adding a CAES system would always result in a loss of revenues for Italy. Therefore, for Moldova and Sweden, it is better to buy more electricity to compress the air (Cases 2 and 2-T). Case 2-T is the best and Case 3 the worst in these countries. For Moldova, only Case 2-T can provide significant relative energy savings (+3.3 %), while for Sweden, both Cases 2 and 2-T provide good results, with energy savings of +2.8 % and +4.4 %, where the increment of 1.6 % is due to the Tesla turbine. Sweden has the highest total daily cost, but in Case 2-T, it also has the highest daily savings and relative daily savings compared to all other cases, meaning that this technology has more potential for implementation in this country. For Italy, in this scenario there is always a loss when integrating the CAES system, which increases by increasing the electricity bought from the grid.

5.2. Electrical energy for the storage charge taken from an excess of RES

The CAES system always provides relative economic savings when

Table 4
Configurations description.

Case identifier	First 12 h (off-peak hours)	Second 12 h (core hours)
Case: 1 (baseline)	40 kW satisfied by the mGT only	80 kW satisfied by the mGT only
Case: 2	40 kW satisfied by the mGT only, while CAES is charging	80 kW satisfied by the mGT, while CAES is discharging
Case: 2 - T	40 kW satisfied by the mGT only, while CAES is charging	80 kW satisfied by the mGT and Tesla turbine, while CAES is discharging
Case: 3	40 kW satisfied by the mGT, while CAES is discharging	80 kW satisfied by the mGT only, while CAES is charging
Case: 3 - T	40 kW satisfied by the mGT and Tesla turbine, while CAES is discharging	80 kW satisfied by the mGT only, while CAES is charging

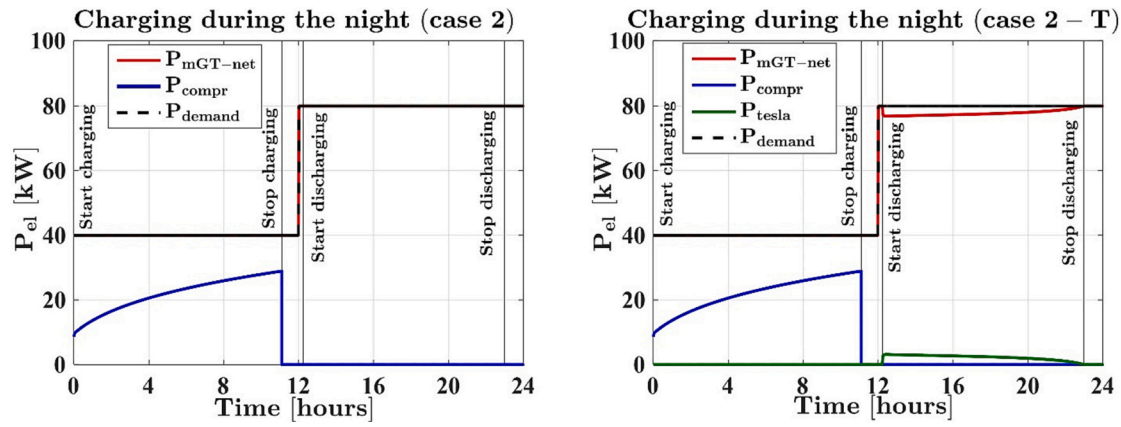


Fig. 5. Power demand, power absorbed by the compressor and generated by the mGT and Tesla turbine for cases 2 (left) and 2-T (right).

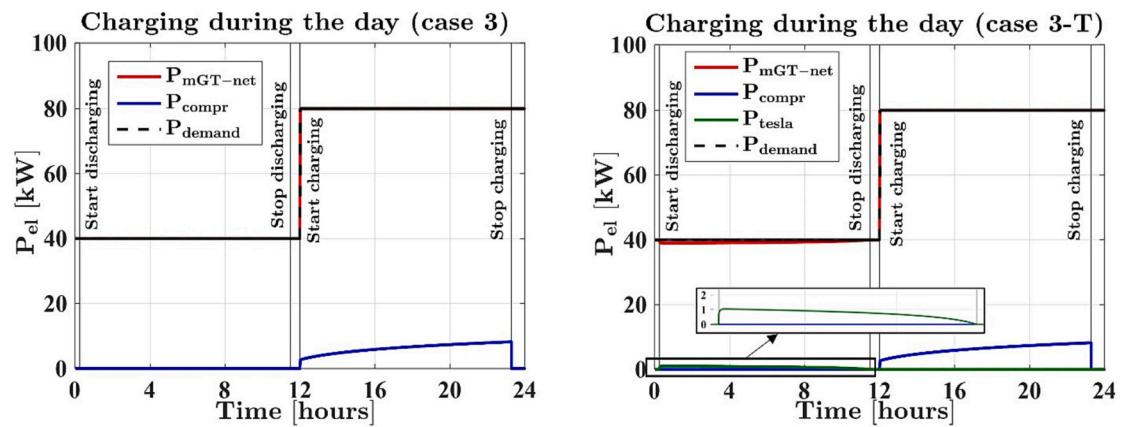


Fig. 6. Power demand, power absorbed by the compressor and generated by the mGT and Tesla turbine for cases 3 (left) and 3-T (right).

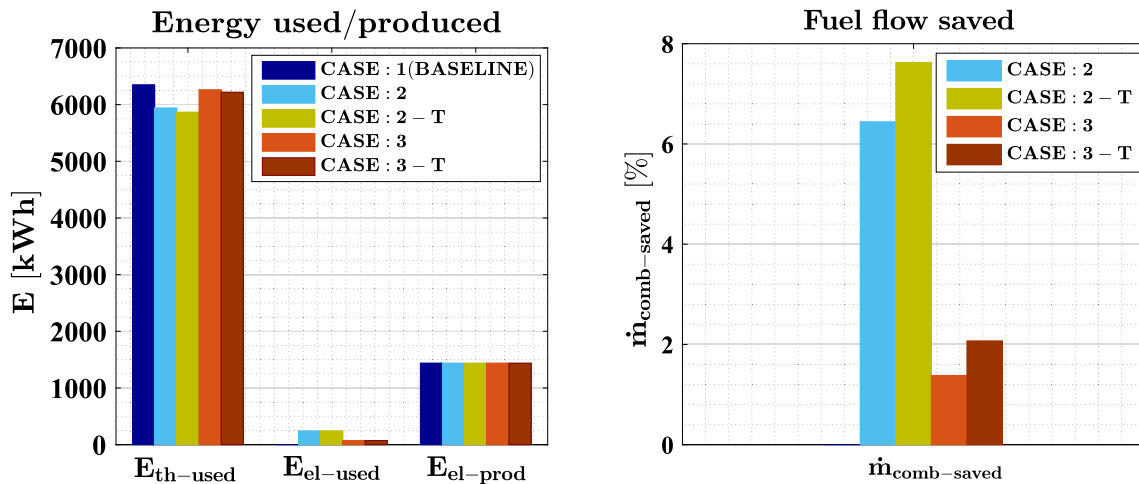


Fig. 7. Energy used and produced comparison (left) and fuel flow saved (right).

Table 5
Electricity and natural gas cost for the first semester of 2022 [50,51].

Country	El. cost [€/kWh]	Fuel cost [€/kWh]
Italy	0.3115	0.0986
Moldova	0.1172	0.0842
Sweden	0.2525	0.2216

using excess renewable energy sources, especially when fuel prices are high (Table 7). The results show that Case 2-T provides the highest daily savings and Case 3 the lowest compared to the baseline in all three countries. Therefore, in all the countries, significant benefits are obtained when injecting the maximum mass flow rate of 50 g/s at 80 kW with the expansion in the Tesla turbine. The daily and relative daily savings (in this scenario) compared to the baseline are also graphically reported in Fig. 9. For Italy, compared to the previous case, higher

Table 6
Daily costs and earnings when purchasing electricity from the grid.

Case identifier		Daily fuel cost	Daily electricity cost	Daily-earnings	Total daily cost	Daily savings	Relative daily savings
		[€/day]	[€/day]	[€/day]	[€/day]	[€/day]	[%]
Italy	Case: 1 (baseline)	626.2	0.0	448.5	177.8	–	–
	Case: 2	585.9	75.9	448.5	213.3	–35.6	–20.0
	Case: 2 - T	578.5	75.9	448.5	205.9	–28.2	–15.8
	Case: 3	617.6	22.2	448.5	191.3	–13.5	–7.6
Moldova	Case: 3 - T	613.2	22.2	448.5	187.0	–9.2	–5.2
	Case: 1 (baseline)	534.8	0.0	168.7	366.0	–	–
	Case: 2	500.3	28.6	168.7	360.1	+5.9	+1.6
	Case: 2 - T	494.0	28.6	168.7	353.8	+12.2	+3.3
Sweden	Case: 3	527.4	8.3	168.7	367.0	–1.0	–0.3
	Case: 3 - T	523.7	8.3	168.7	363.3	+2.7	+0.7
	Case: 1 (baseline)	1407.4	0.0	363.5	1043.9	–	–
	Case: 2	1316.7	61.5	363.5	1014.7	+29.2	+2.8
	Case: 2 - T	1300.1	61.5	363.5	998.1	+45.8	+4.4
	Case: 3	1388.0	18.0	363.5	1042.4	+1.5	+0.1
	Case: 3 - T	1378.3	18.0	363.5	1032.7	+11.2	+1.1

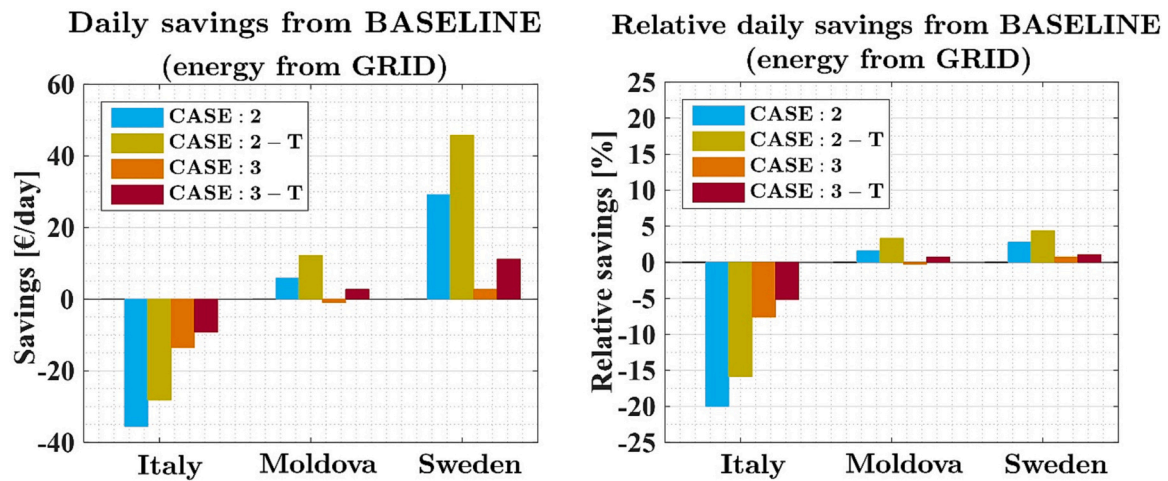


Fig. 8. Daily savings compared to the baseline case when energy is bought from the grid.

Table 7
Daily costs and earnings when using an excess of renewables.

Case identifier		Daily fuel cost	Daily electricity cost	Daily-earnings	Total daily cost	Daily savings	Relative daily savings
		[€/day]	[€/day]	[€/day]	[€/day]	[€/day]	[%]
Italy	Case: 1 (baseline)	626.2	0.0	448.5	177.8	–	–
	Case: 2	585.9	0.0	448.5	137.4	+40.4	+22.7 %
	Case: 2 - T	578.5	0.0	448.5	130.0	+47.8	+26.9 %
	Case: 3	617.6	0.0	448.5	169.1	+8.7	+4.9 %
Moldova	Case: 3 - T	613.2	0.0	448.5	164.8	+13.0	+7.3 %
	Case: 1 (baseline)	534.8	0.0	168.7	366.0	–	–
	Case: 2	500.3	0.0	168.7	331.6	+34.5	+9.4 %
	Case: 2 - T	494.0	0.0	168.7	325.3	+40.8	+11.1 %
Sweden	Case: 3	527.4	0.0	168.7	358.6	+7.4	+2.0 %
	Case: 3 - T	523.7	0.0	168.7	355.0	+11.1	+3.0 %
	Case: 1 (baseline)	1407.4	0.0	363.5	1043.9	–	–
	Case: 2	1316.7	0.0	363.5	953.2	+90.7	+8.7 %
	Case: 2 - T	1300.1	0.0	363.5	936.6	+107.3	+10.3 %
	Case: 3	1388.0	0.0	363.5	1024.5	+19.4	+1.9 %
	Case: 3 - T	1378.3	0.0	363.5	1014.7	+29.2	+2.8 %

relative daily savings (+22.7 % for Case 2-T) can be obtained due to the lower daily total cost. In absolute values, the daily savings for Moldova are the lowest and for Sweden the highest (Fig. 9, left). However, they have comparable relative daily savings as Moldova's total daily costs are lower than those of Sweden.

6. Dynamic analysis

This paragraph investigates the influence of the injection of air and load change during CAES discharging on the dynamic performance of the mGT. The second configuration, with a tank size of $V_{\text{tank}} = 40 \text{ m}^3$, has been chosen for its higher economic potential. Different representative possible transient scenarios have been considered when operating

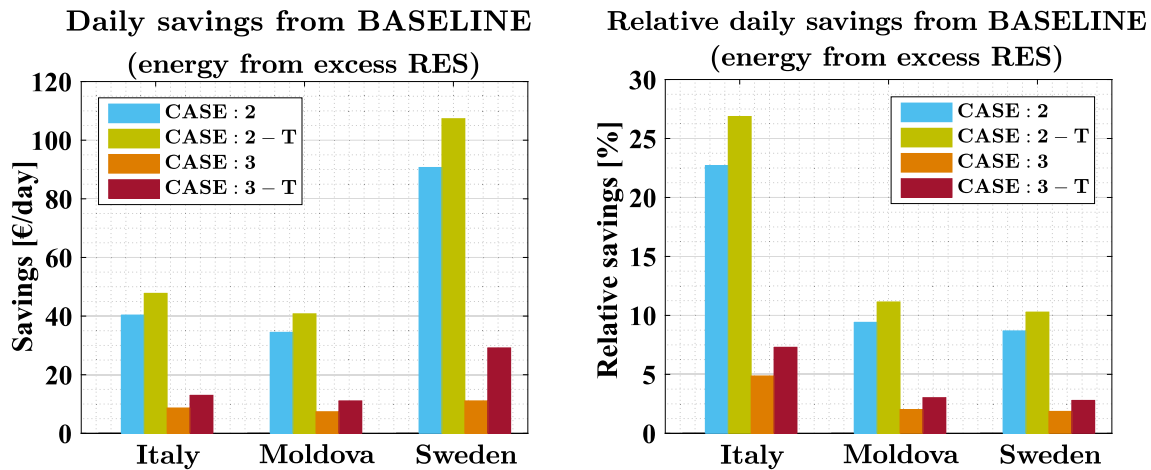


Fig. 9. Daily savings compared to the baseline case when energy is taken from excess renewables.

with a CAES system:

1. Step injections of compressed air at constant power (for $P_{net} = 40$ kW and $P_{net} = 80$ kW)
2. Step and gradual injections at constant power (for $P_{net} = 80$ kW)
3. Step and gradual stop of injections at constant power (for $P_{net} = 80$ kW)
4. Step injection with gradual power output variation from 40 kW to 80 kW

Each case starts from a stable condition at $t = 0$ s, while the operating conditions change begins at $t = 100$ s.

6.1. Step injections of compressed air at constant power (for $P_{net} = 40$ kW and $P_{net} = 80$ kW)

The effect of compressed air injection at constant power output was considered for a lower ($P_{net} = 40$ kW) and higher load ($P_{net} = 80$ kW). More air can be injected at a higher load since the starting surge margin (without injection) is higher than at a lower load. In both cases, the surge margin is initially reduced during the injection before reaching stable conditions (Fig. 10). This effect is more noticeable at $P_{net} = 80$ kW and leads to a reduction of k_p below 1.1 when $\dot{m}_{inj} = 50$ g/s is injected, acceptable solution considering the steady-state results. This reduction is due to the control system action: when the air is injected, the power

output initially increases, the control system reduces the rotational speed and, therefore, the compressor mass flow reduces with a fast response, while the pressure ratio remains high for a longer time before reducing as well. In detail, the pressure ratio initially increases before settling since the initial reduction of the TOT, due to the air injection, leads the control system to initially increase the fuel flow. This also contributes to the initial peak of produced power (Fig. 11). The graphs of Fig. 11 represent the generated power P_{gen} that considers the power used by auxiliaries. The TOT transient behaviour of Fig. 12 shows a peak before stabilising to 645 °C; however, the machine can handle a maximum value of 655 °C for a few seconds and therefore no potential problems due to thermal gradients have been detected.

These results mainly show that 50 g/s of air injection step is not acceptable at high load and 15 g/s of air injection step could be critical at low load, because an oscillation too close to the surge margin limit could be a risk. Since this significantly reduces the operating margin in comparison with the steady-state results, a real application needs a different approach, to avoid the diminution of the positive impact in terms of cost decrease and efficiency increase.

6.2. Step and gradual injections at constant power (for $P_{net} = 80$ kW)

Due to the critical dynamic behaviour when injecting the maximum allowed injection rate obtained for the steady-state conditions, different injection ramps were considered by progressively reducing the rate of

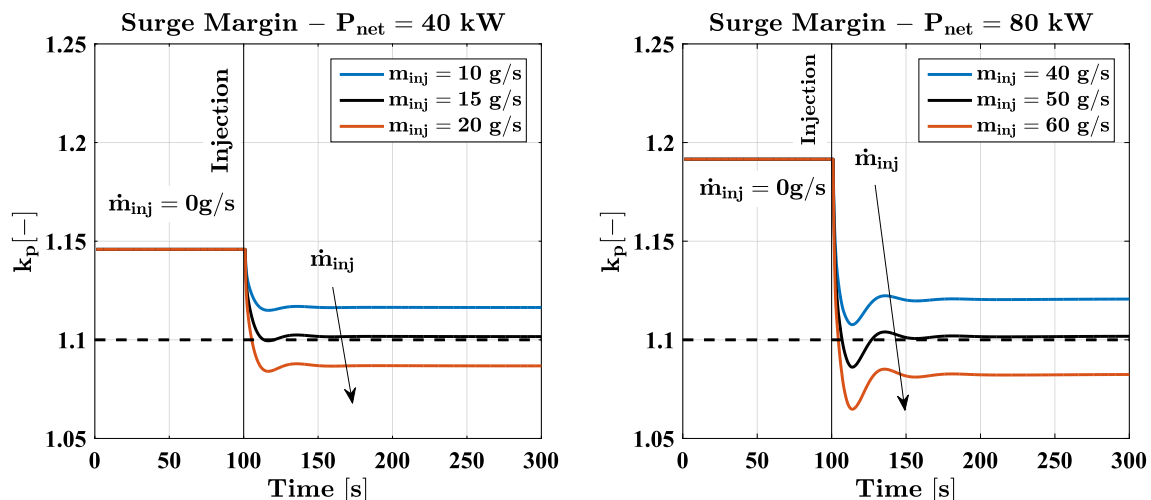


Fig. 10. Surge margin variation when injecting compressed air at $P_{net} = 40$ kW (left) and 80 kW (right).

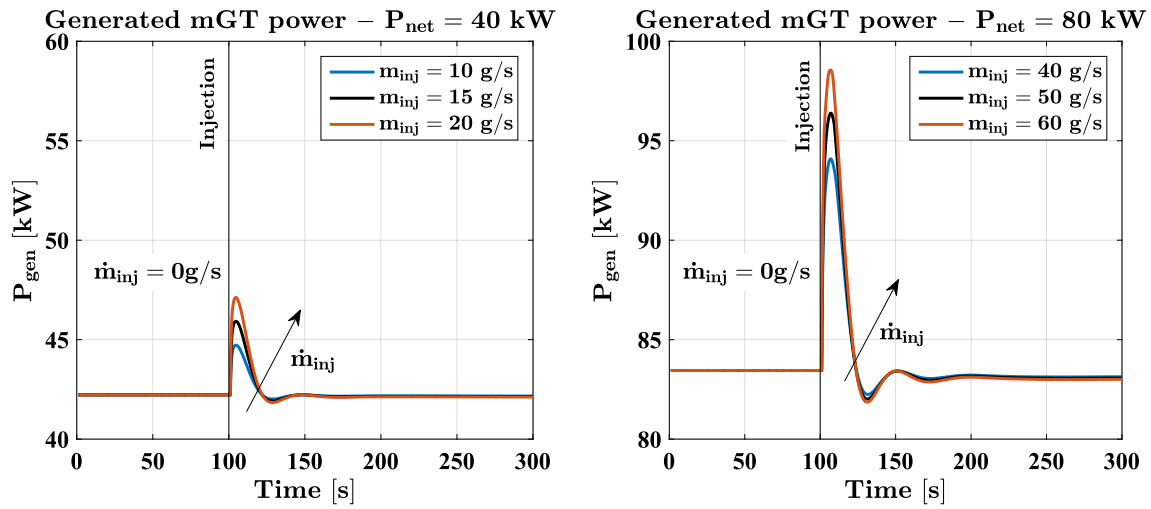


Fig. 11. Generated mGT power variation when injecting compressed air at $P_{net} = 40$ kW (left) and 80 kW (right).

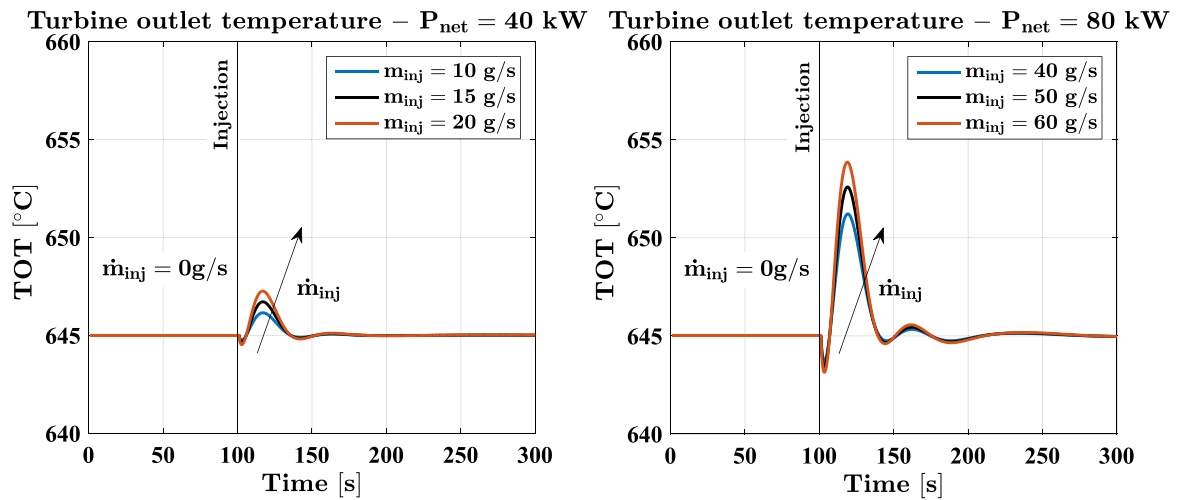


Fig. 12. TOT variation when injecting compressed air at $P_{net} = 40$ kW (left) and 80 kW (right).

injection (Fig. 13). This could be an important solution (coming from this dynamic analysis) to be implemented in a real CAES/mGT system. The case with $P_{net} = 80$ kW was chosen for this analysis as being the

most critical. For example, with a rate of $+0.5$ (g/s)/s, it is always possible to ensure $k_p > 1.1$. Reducing the injection rate allows the k_p to keep within the acceptable limits and, therefore, to introduce a higher

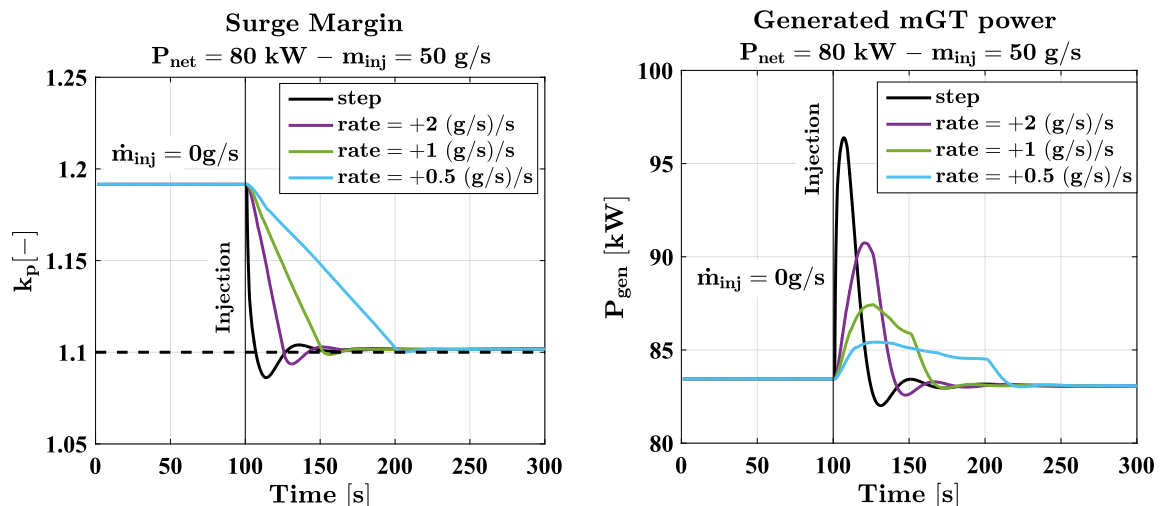


Fig. 13. Surge margin (left) and generated mGT power (right) for step and gradual injections at constant power (for $P_{net} = 80$ kW).

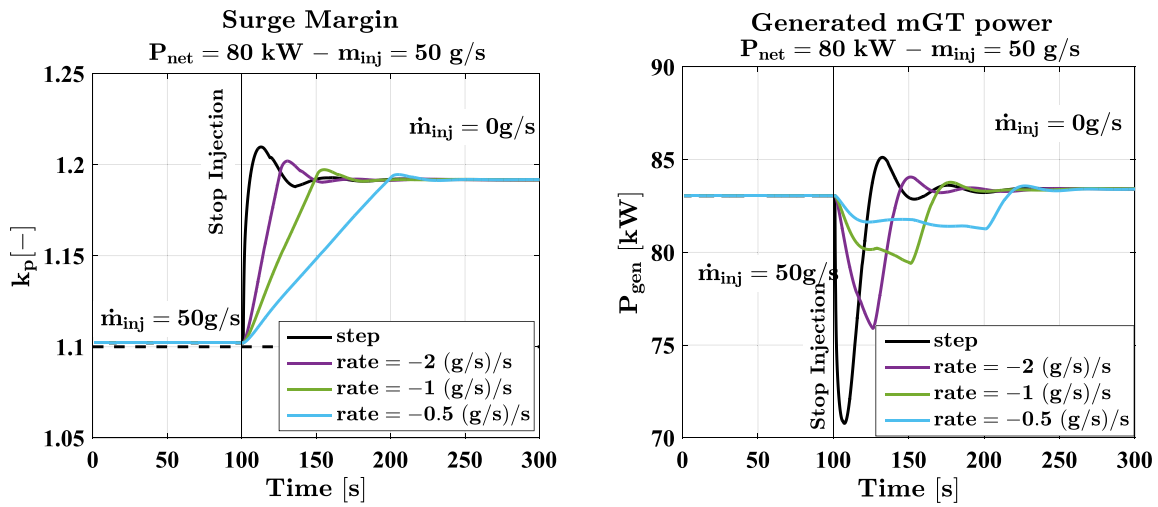


Fig. 14. Surge margin (left) and generated mGT power (right) for step and gradual stop of injections at constant power (for $P_{net} = 80$ kW).

mass flow of injected air, benefiting the system overall performance. This also reduces the power and TOT oscillations with a smoother transition to the steady-state condition. Since the generated power peak is also reduced, more stable power output is provided to the grid. So, with the proposed ramp, a real commercial AE-T100 could be used in the full operative range defined in the steady-state analysis without further limitations.

6.3. Step and gradual stop of injections at constant power (for $P_{net} = 80$ kW)

Even though less critical, the dynamic behaviour where the injection is stopped is also worth studying. During the stop of the air injection, an opposite transient behaviour can be noticed (Fig. 14). The surge margin and TOT values are never critical, even when the air injection suddenly stops. However, considering the produced power, in this case too, a beneficial effect can be shown when gradually reducing the injected air to ensure a more stable power production. Also in this case, the proposed ramp for removing the air injection is a positive solution to decrease the stress on the commercial machine extending the component duration.

6.4. Step injection with gradual power output variation from 40 kW to 80 kW

A final case is investigated, where a power output variation coincides with the start of the injection. In this case (see Fig. 15), the injection was performed with a step of 50 g/s while the power output was gradually changed from 40 kW to 80 kW with a ramp of 1 min. The surge margin plot shows that there is a significant reduction. This demonstrates that the injection schedule should not be performed during critical power change variations and a waiting time should be considered. This is an important result to be applied in a real system because a waiting time (between the power and the air injection variations) of at least 2–3 mins can prevent the superimposition of two transient operations and avoid the machine failure.

7. Conclusions

This paper presents a dynamic analysis on an AE-T100 micro gas turbine coupled with a small-size second-generation CAES system. It consists of a two-stage reciprocating compressor with intercooling and aftercooling, an artificial vessel for storing compressed air and an additional recuperator for air pre-heating. The application of a Tesla turbine placed after the storage vessel is also investigated for additional power recovery. The main results obtained in this work allow to extend

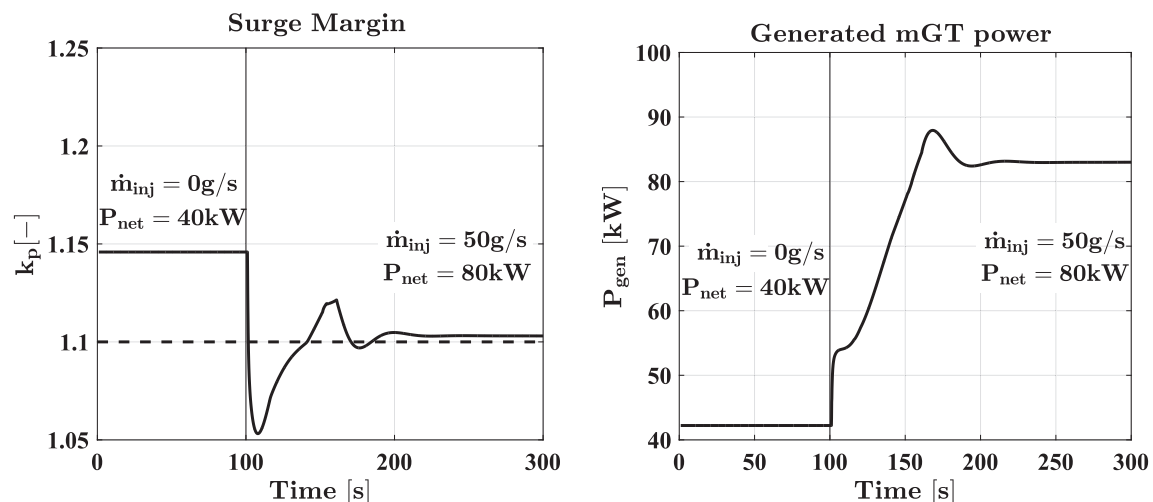


Fig. 15. Surge margin (left) and generated mGT power (right) for step injection with gradual power output variation from 40 kW to 80 kW.

the AE-T100 applications in a CAES system with the following positive impacts on energy sustainability: efficiency increase, fuel consumption decrease, energy cost decrease, flexible energy storage for renewable sources. Special attention is focused on the calculation of the system integration constraints to prevent risks for the microturbine also in dynamic conditions and the related definition of operating procedures (ramps instead of steps) to enlarge the system flexibility to the maximum limits in terms of air flows injected in the AE-T100 ducts.

The analysis begins with a steady-state study examining the micro gas turbine behaviour when injecting compressed air at different part-load conditions. This analysis estimated the maximum mass flow rate that could be injected into the micro gas turbine at different power outputs, ensuring safe operation of the compressor. This showed that higher mass flow rates can be injected at higher power outputs. For example, at $P_{net} = 80$ kW, the maximum mass flow rate is $\dot{m}_{inj} = 50$ g/s resulting in an increment of the electrical efficiency of +3.23 %, while at $P_{net} = 40$ kW, the maximum mass flow for discharge is $\dot{m}_{inj} = 15$ g/s allowing a +0.76 % of increment in efficiency.

The dynamic analysis of the micro gas turbine when operated with a compressed air energy storage (CAES) system is conducted and results show that the surge margin is reduced during the step injection before reaching stable conditions, even in conditions acceptable for steady-state operations. The reduction is more pronounced at a higher load and injection rates. Hence this analysis calculated that, considering injection steps, 50 g/s of air injection is not acceptable at high load and 15 g/s of air injection could be critical at low load, due to an oscillation too close to the surge margin limit. However, operating injection ramps instead of steps is a solution to keep the surge margin within acceptable limits and reduce power and TOT oscillations. In details, a rate of +0.5 (g/s)/s was calculated as a good compromise to operate the micro-turbine changes safely and fast in dynamic mode, without reducing the operating range related to the steady-state calculations.

Finally, the results obtained in this work will be important to manage this mGT/CAES system for commercial applications, avoiding dangerous operating procedures and situations, and proposing a calculation approach that can be repeated in case of other types of micro-turbines. In details, the definition of the air injection constraints and the ramp rates for safe operations allows to extend the system operative range to the calculated limits with a positive impact on the flexibility and the energy sustainability issues (fuel consumption decrease and flexibility increase for the variability compensation of renewable sources and the related positive impact on pollution and energy cost decrease).

Nomenclature

Acronyms

A-CAES	Adiabatic CAES
AE-T100	Ansaldo Energia T100
CAES	Compressed Air Energy Storage
CHP	Combined Heat and Power
D-CAES	Diabatic CAES
DER	Distributed Energy Resource
DHN	District Heating Network
ESS	Energy Storage Systems
I-CAES	Isothermal CAES
MG	Microgrid
mGT	micro Gas Turbine
NextMGT	Next Generation of Micro Gas Turbines for High Efficiency, Low Emissions, and Fuel Flexibility
OPEX	Operating Expense
PI	Proportional Integral
PID	Proportional Integral Derivative
RES	Renewable Energy Source

S-CAES	Second Generation CAES
TES	Thermal Energy Storage
TOT	Turbine Outlet Temperature
TPG	Thermochemical Power Group
VUB	Vrije Universiteit Brussel

Variables

\dot{q}	heat flux
A	area
C	momentum contribution
D	diameter
c_p	specific heat at constant pressure
c_v	specific heat at constant volume
f	friction coefficient
h	enthalpy
J	rotational inertia
k_p	surge margin
L	total length
LHV	Low heating value
M	mass
\dot{m}	mass flow rate
N	rotational speed
p	pressure
P	power
T	temperature
v	velocity
V	volume
x	discretised axial length

Greek symbols

ρ	density
η	efficiency
β	pressure ratio
γ	ratio of the specific heats at constant pressure and volume
Δ	delta
ω	angular rotational speed

Subscripts

air	referred to air properties
charge	referred to the charging phase
cold	cold side
comb	combustor
compr	compressor
el	electrical
eq	equivalent
fuel	referred fuel
gas	referred to gas properties
gen	generated
hot	hot side
i	i-th element in the discretisation
in	referred to inlet properties
inj	referred to the injection phase
j	j-th element in the discretisation
loss	losses
m	mechanical
max	maximum
mean	referred to average properties
net	net
out	referred to outlet properties
pipe	pipe
rec	recuperator
s.l.	surge line
solid	referred to the solid part

tank referred to the storage tank
 th thermal
 turb turbine


Declaration of competing interest

The authors declare that they have no known competing financial interests or personal relationships that could have appeared to influence the work reported in this paper.

Data availability

Data will be made available on request.

Acknowledgements

This project has received funding from the European Union's Horizon 2020 research and innovation programme  under the Marie Skłodowska-Curie grant agreement No 861079 ("NextMGT - Next Generation of Micro Gas Turbines for High Efficiency, Low Emissions, and Fuel Flexibility"). This paper reflects only the authors' view and the Research Executive Agency and the European Commission are not responsible for any use that may be made of the information it contains.

References

- [1] IEA, Renewable Energy Market Update-May 2022, 2022, <https://doi.org/10.1787/faf30e5a-en>.
- [2] A.Q. Al-Shetwi, M.A. Hannan, K.P. Jern, M. Mansur, T.M.I. Mahlia, Grid-connected renewable energy sources: review of the recent integration requirements and control methods, *J. Clean. Prod.* 253 (2020), 119831, <https://doi.org/10.1016/j.jclepro.2019.119831>.
- [3] D. Bellotti, M. Rivarolo, L. Magistri, A comparative techno-economic and sensitivity analysis of Power-to-X processes from different energy sources, *Energy Convers. Manag.* 260 (2022), 115565, <https://doi.org/10.1016/j.enconman.2022.115565>.
- [4] W. Wang, B. Yuan, Q. Sun, R. Wennersten, Application of energy storage in integrated energy systems—a solution to fluctuation and uncertainty of renewable energy, *J. Energy Storage.* 52 (2022), 104812, <https://doi.org/10.1016/j.est.2022.104812>.
- [5] M. Cavo, M. Rivarolo, L. Gini, L. Magistri, An advanced control method for fuel cells - metal hydrides thermal management on the first Italian hydrogen propulsion ship, *Int. J. Hydrogen Energy.* (2022), <https://doi.org/10.1016/j.ijhydene.2022.07.223>.
- [6] M. Rivarolo, D. Rattazzi, L. Magistri, A.F. Massardo, Multi-criteria comparison of power generation and fuel storage solutions for maritime application, *Energy Convers. Manag.* 244 (2021), 114506, <https://doi.org/10.1016/j.enconman.2021.114506>.
- [7] D. Zhang, G.M. Shafiullah, C.K. Das, K.W. Wong, A systematic review of optimal planning and deployment of distributed generation and energy storage systems in power networks, *Journal of Energy Storage.* 56 (2022), 105937, <https://doi.org/10.1016/j.est.2022.105937>.
- [8] M.F. Akorede, H. Hizam, E. Pournesmael, Distributed energy resources and benefits to the environment, *Renew. Sustain. Energy Rev.* 14 (2010) 724–734, <https://doi.org/10.1016/j.rser.2009.10.025>.
- [9] H. Jiayi, J. Chuanwen, X. Rong, A review on distributed energy resources and MicroGrid, *Renew. Sustain. Energy Rev.* 12 (2008) 2472–2483, <https://doi.org/10.1016/j.rser.2007.06.004>.
- [10] A. Bouakkaz, A.J.G. Mena, S. Haddad, M.L. Ferrari, Efficient energy scheduling considering cost reduction and energy saving in hybrid energy system with energy storage, *J. Energy Storage.* 33 (2021), 101887, <https://doi.org/10.1016/j.est.2020.101887>.
- [11] O. Krishan, S. Suhag, An updated review of energy storage systems: classification and applications in distributed generation power systems incorporating renewable energy resources, *Int. J. Energy Res.* 43 (2019) 6171–6210, <https://doi.org/10.1002/er.4285>.
- [12] A. Gil, M. Medrano, I. Martorell, A. Lázaro, P. Dolado, B. Zalba, L.F. Cabeza, State of the art on high temperature thermal energy storage for power generation. Part 1—concepts, materials and modellization, *Renewable and Sustainable Energy Reviews* 14 (2010) 31–55, <https://doi.org/10.1016/j.rser.2009.07.035>.
- [13] C.R. Matos, P.P. Silva, J.F. Carneiro, Overview of compressed air energy storage projects and regulatory framework for energy storage, *J. Energy Storage.* 55 (2022), 105862, <https://doi.org/10.1016/j.est.2022.105862>.
- [14] A.L. Facci, D. Sánchez, E. Jannelli, S. Ubertini, Trigenerative micro compressed air energy storage: concept and thermodynamic assessment, *Appl. Energy.* 158 (2015) 243–254, <https://doi.org/10.1016/j.apenergy.2015.08.026>.
- [15] Alvaro De Gracia, Luisa F. Cabeza, Phase change materials and thermal energy storage for buildings, *Energy and Buildings* 103 (2015) 414–419, <https://doi.org/10.1016/j.enbuild.2015.06.007>.
- [16] G. Dib, P. Haberschild, R. Rullière, R. Revellin, Modelling small-scale trigenerative advanced adiabatic compressed air energy storage for building application, *Energy* 237 (2021), <https://doi.org/10.1016/j.energy.2021.121569>.
- [17] C. Salvini, Performance analysis of small size compressed air energy storage systems for power augmentation: air injection and air injection/expander schemes, *Heat Transf. Eng.* 39 (2018) 304–315, <https://doi.org/10.1080/01457632.2017.1295746>.
- [18] J. Zhang, S. Zhou, S. Li, W. Song, Z. Feng, Performance analysis of diabatic compressed air energy storage (D-CAES) system, *Energy Procedia* 158 (2019) 4369–4374, <https://doi.org/10.1016/j.egypro.2019.01.782>.
- [19] Y. Tian, T. Zhang, N. Xie, Z. Dong, Z. Yu, M. Lyu, Y. Lai, X. Xue, Conventional and advanced exergy analysis of large-scale adiabatic compressed air energy storage system, *J. Energy Storage* 57 (2023), 106165, <https://doi.org/10.1016/j.est.2022.106165>.
- [20] T. Kim, C. Lee, Y. Hwang, R. Radermacher, A review on nearly isothermal compression technology, *Int. J. Refrig.* 144 (2022) 145–162, <https://doi.org/10.1016/j.ijrefrig.2022.07.008>.
- [21] R. Li, R. Tao, X. Feng, E. Yao, H. Zhang, L. Ling, H. Wang, Energy distributing and thermodynamic characteristics of a coupling near-isothermal compressed air energy storage system, *J. Energy Storage* 58 (2023), 106314, <https://doi.org/10.1016/j.est.2022.106314>.
- [22] G.L. Arnulfi, G. Croce, Compressed air energy storage for a small size standalone plant powered by a solar power unit and a gas turbine, *Proc. ASME Turbo Expo.* 5 (2020) 1–10, <https://doi.org/10.1115/GT2020-14631>.
- [23] C. Salvini, Techno-economic analysis of small size second generation CAES system, *Energy Procedia* 82 (2015) 782–788, <https://doi.org/10.1016/j.egypro.2015.11.812>.
- [24] P.A. Pilavachi, Mini- and micro-gas turbines for combined heat and power, *Appl. Therm. Eng.* 22 (2002) 2003–2014, [https://doi.org/10.1016/S1359-4311\(02\)00132-1](https://doi.org/10.1016/S1359-4311(02)00132-1).
- [25] B. Bazooyar, H.G. Darabkhani, Design and numerical analysis of a 3 kWe flameless microturbine combustor for hydrogen fuel, *International Journal of Hydrogen Energy* 44 (2019) 11134–1114423, <https://doi.org/10.1016/j.ijhydene.2019.02.132>.
- [26] C.D. Ávila, S. Cardona, M. Abdullah, T.F. Guiberti, W.L. Roberts, Experimental assessment of the performance of a commercial micro gas turbine fueled by ammonia-methane blends, *Applications in Energy and Combustion Science* 13 (2023), 100104, <https://doi.org/10.1016/j.jaacs.2022.100104>.
- [27] X. Wang, C. Yang, M. Huang, X. Ma, Multi-objective optimization of a gas turbine-based CCHP combined with solar and compressed air energy storage system, *Energy Convers. Manag.* 164 (2018) 93–101, <https://doi.org/10.1016/j.enconman.2018.02.081>.
- [28] J. Zhang, K.J. Li, M. Wang, W.J. Lee, H. Gao, C. Zhang, K. Li, A bi-level program for the planning of an islanded microgrid including CAES, *IEEE Trans. Ind. Appl.* 52 (2016) 2768–2777, <https://doi.org/10.1109/TIA.2016.2539246>.
- [29] M.J. Ghadi, A. Azizivahed, D.K. Mishra, L. Li, J. Zhang, M. Shafie-khah, J.P. S. Catalão, Application of small-scale compressed air energy storage in the daily operation of an active distribution system, *Energy* 231 (2021), <https://doi.org/10.1016/j.energy.2021.120961>.
- [30] H. Jin, P. Liu, Z. Li, Dynamic modeling and design of a hybrid compressed air energy storage and wind turbine system for wind power fluctuation reduction, *Comput. Chem. Eng.* 122 (2019) 59–65, <https://doi.org/10.1016/j.compchemeng.2018.05.023>.
- [31] S. Mucci, A. Bischi, S. Briola, A. Baccioli, Small-scale adiabatic compressed air energy storage: control strategy analysis via dynamic modelling, *Energy Convers. Manag.* 243 (2021), 114358, <https://doi.org/10.1016/j.enconman.2021.114358>.
- [32] J.-M. Fafara, N. Modliński, Numerical study of internal flue gas recirculation system applied to methane-hydrogen powered gas microturbine combustor, *Combustion Engines* 192 (2023), <https://doi.org/10.19206/CE-152236>.
- [33] G. Xiao, J. Yang, D. Ni, Model predictive control of a solar power system with microturbine and thermochemical energy storage, *Industrial and Engineering Chemistry Research* 61 (2022) 13532–13558, <https://doi.org/10.1021/acs.iecr.2c01784>.
- [34] X. Zhang, Y. Li, Z. Gao, S. Chen, Y. Xu, H. Chen, Overview of dynamic operation strategies for advanced compressed air energy storage, *Journal of Energy Storage* 66 (2023), 107408, <https://doi.org/10.1016/j.est.2023.107408>.
- [35] H. Mozayeni, X. Wang, M. Negnevitsky, Dynamic analysis of a low-temperature Adiabatic Compressed Air Energy Storage system, *Journal of Cleaner Production* 276 (2020), 124323, <https://doi.org/10.1016/j.jclepro.2020.124323>.
- [36] L. Chen, L. Zhang, H. Yang, M. Xie, K. Ye, Dynamic simulation of a re-compressed adiabatic compressed air energy storage (RA-CAES) system, *Energy* 261 (2022), 125351, <https://doi.org/10.1016/j.energy.2022.125351>.
- [37] Q. Xu, Y. Wu, W. Zheng, Y. Gong, S. Dubljevic, Modeling and dynamic safety control of compressed air energy storage system, *Renewable Energy* 208 (2023) 203–213, <https://doi.org/10.1016/j.renene.2023.03.011>.
- [38] J. Huang, Y. Xu, H. Guo, X. Geng, H. Chen, Dynamic performance and control scheme of variable-speed compressed air energy storage, *Applied Energy* 325 (2022), 119338, <https://doi.org/10.1016/j.apenergy.2022.119338>.

- [39] A. Renuke, A. Traverso, M. Pascenti, Experimental campaign tests on a Tesla micro-expanders, E3S Web Conf. 113 (2019) 1–9, <https://doi.org/10.1051/e3sconf/201911303015>.
- [40] A. Renuke, A. Traverso, Performance assessment of Tesla expander using three-dimensional numerical simulation, Journal of Engineering for Gas Turbines and Power 144 (2022), 111006, <https://doi.org/10.1115/1.4055486>.
- [41] A. Traverso, TRANSEO code for the dynamic performance simulation of micro gas turbine cycles, in: Proc. ASME Turbo Expo, 2005, <https://doi.org/10.1115/GT2005-68101>.
- [42] Turbec, T100 Microturbine System: Technical Description, 2009, p. 17.
- [43] A. Traverso, F. Calzolari, A. Massardo, Transient analysis of and control system for advanced cycles based on micro gas turbine technology, J. Eng. Gas Turbines Power 127 (2005) 340–347, <https://doi.org/10.1115/1.1839918>.
- [44] J. Chen, G. Xiao, M.L. Ferrari, T. Yang, M. Ni, Dynamic simulation of a solar-hybrid microturbine system with experimental validation of main parts, Renew. Energy 154 (2020) 187–200, <https://doi.org/10.1016/j.renene.2019.11.022>.
- [45] M. Mahmood, A. Traverso, A. Nicola, A.F. Massardo, D. Marsano, C. Cravero, Thermal energy storage for CSP hybrid gas turbine systems: dynamic modelling and experimental validation, Applied Energy 212 (2018) 1240–1251, <https://doi.org/10.1016/j.apenergy.2017.12.130>.
- [46] L. Larosa, A. Traverso, A.F. Massardo, Dynamic analysis of a recuperated mgt cycle for fuel cell hybrid systems, in: Proc. ASME Turbo Expo, American Society of Mechanical Engineers (ASME), 2016, <https://doi.org/10.1115/GT2016-57312>.
- [47] M. Montero Carrero, M.L. Ferrari, W. De Paepe, A. Parente, S. Bram, F. Contino, Transient simulations of a T100 micro gas turbine converted into a micro humid air turbine, in: Proc. ASME Turbo Expo 2015, 2015, pp. 1–9, <https://doi.org/10.1115/GT2015-43277>.
- [48] M. Sk, C. Actions, I.T. Networks, N. Generation, M.G. Turbines, H. Efficiency, L. Emissions, F. Flexibility, D. No, Innovative Training Networks (ITN) 861079 – NextMGT (Next Generation of Micro Gas Turbines for High Efficiency, Low Emissions and Fuel Flexibility) Innovation in Heat Exchanger Design for MGTs Including Energy Storage, 2022, pp. 38–44. https://nextmgt.com/wp-content/uploads/2022/12/861079_Deliverable_18_Summary-report-on-innovation-in-heat-exchangers.pdf.
- [49] A. Traverso, A.F. Massardo, R. Scarpellini, Externally fired micro-gas turbine: modelling and experimental performance, Appl. Therm. Eng. 26 (2006) 1935–1941, <https://doi.org/10.1016/j.applthermaleng.2006.01.013>.
- [50] Gas prices for household consumers - bi-annual data (from 2007 onwards), (n.d.). https://ec.europa.eu/eurostat/databrowser/view/nrg_pc_202/default/table?lang=en.
- [51] Electricity prices for household consumers - bi-annual data (from 2007 onwards), (n.d.). https://ec.europa.eu/eurostat/databrowser/view/nrg_pc_204/default/table?lang=en.